Current Biology 24, 845–851, April 14, 2014 ©2014 Elsevier Ltd All rights reserved http://dx.doi.org/10.1016/j.cub.2014.03.008

Report

The Vasa Homolog RDE-12 Engages Target mRNA and Multiple Argonaute Proteins to Promote RNAi in *C. elegans*

Masaki Shirayama,[1,2,3] William Stanney III,[1,2] Weifeng Gu,[1,2,4] Meetu Seth,[1,2,3] and Craig C. Mello[1,2,3,*]
[1]Program in Molecular Medicine
[2]RNA Therapeutics Institute
[3]Howard Hughes Medical Institute
University of Massachusetts Medical School, 368 Plantation Street, Worcester, MA 01605, USA

Summary

Argonaute (AGO) proteins are key nuclease effectors of RNAi [1]. Although purified AGOs can mediate a single round of target RNA cleavage in vitro, accessory factors are required for small interfering RNA (siRNA) loading and to achieve multiple-target turnover [2, 3]. To identify AGO cofactors, we immunoprecipitated the *C. elegans* AGO WAGO-1, which engages amplified small RNAs during RNAi [4]. These studies identified a robust association between WAGO-1 and a conserved Vasa ATPase-related protein RDE-12. *rde-12* mutants are deficient in RNAi, including viral suppression, and fail to produce amplified secondary siRNAs and certain endogenous siRNAs (endo-siRNAs). RDE-12 colocalizes with WAGO-1 in germline P granules and in cytoplasmic and perinuclear foci in somatic cells. These findings and our genetic studies suggest that RDE-12 is first recruited to target mRNA by upstream AGOs (RDE-1 and ERGO-1), where it promotes small RNA amplification and/or WAGO-1 loading. Downstream of these events, RDE-12 forms an RNase-resistant (target mRNA-independent) complex with WAGO-1 and may thus have additional functions in target mRNA surveillance and silencing.

Results and Discussion

The VASA Homolog RDE-12 Is a WAGO-1 Interactor

As in other organisms, the upstream events in the *C. elegans* RNAi response include processing of long double-stranded RNA (dsRNA) into small interfering RNAs (siRNAs) by the RNase III-related protein Dicer, loading of siRNAs into an RNase H-related Argonaute (AGO) protein, and scanning for target mRNAs by siRNA-mediated base pairing that precisely positions AGO for target mRNA cleavage [5]. In *C. elegans*, however, the slicer activity of the primary AGO, RDE-1, is not required for silencing [6]. Instead, through mechanisms that are still largely unknown, RDE-1 recruits RNA-dependent RNA polymerase (RdRP) [7, 8]. RdRP then utilizes the target mRNA as a template for the de novo synthesis of secondary siRNAs (termed 22G-RNAs) [4]. 22G-RNAs are then loaded onto secondary AGOs of the "worm-specific AGO" (WAGO) protein family [4]. WAGO proteins lack catalytic residues thought to be essential for target cleavage [9], and thus silencing is thought to involve the recruitment of unknown accessory factors that mediate mRNA turnover.

Given our incomplete understanding of how AGO proteins mediate key events such as RdRP recruitment and mRNA turnover, we sought to identify proteins that interact with worm AGO proteins in vivo. The WAGO-1 protein is abundantly expressed in germline nuage-like structures called P granules [4]. Previous studies suggest that WAGO-1 functions in both exogenous dsRNA-induced (exo-RNAi) and several endogenous RNAi pathways [4]. To identify WAGO-1 protein interactors, we immunoprecipitated FLAG-tagged WAGO-1 and analyzed the coprecipitated proteins by SDS-PAGE. This analysis identified a 100 kDa protein that coprecipitated with FLAG::WAGO-1 (Figure 1A). Tandem mass spectrometry unambiguously identified this protein as F58G11.2, which is predicted to encode a DEAD box RNA-binding ATPase most similar to Vasa/DDX4 and Belle/DDX3. In addition, F58G11.2 contains two phenylalanine-glycine (FG)-repeat domains that flank the ATPase domain [10] (Figure 2A). Because F58G11.2 is required for RNAi (see below), we refer to *f58g11.2* as *rde-12* (*R*NAi *de*ficient-*12*).

RDE-12-specific antisera recognized a 100 kDa protein in the wild-type that is absent or truncated in *rde-12* mutant animals (Figure 1B). Consistent with our WAGO-1 mass spectrometry findings, RDE-12 protein coimmunoprecipitated FLAG::WAGO-1 (Figure 1C). The interaction between WAGO-1 and RDE-12 was resistant to RNase A treatment, suggesting that the interaction is not bridged by RNA. Interestingly, we found that WAGO-1 and RDE-12 do not coimmunoprecipitate (coIP) in *rde-3* mutants (Figure 1D), where the majority of both endogenous and exogenous secondary siRNAs are absent [4, 11]. RDE-12 IP followed by multidimensional protein identification technology (MudPIT) analysis detected WAGO-1 and a primary AGO, ERGO-1 [12], but failed to detect other AGO proteins (data not shown). The ERGO-1 interaction was confirmed by coIP and immunoblot analysis with a rescuing FLAG::RDE-12 (Figure 1E). FLAG::RDE-12 IP also coprecipitated HA::RDE-1 (Figure 1F), suggesting that RDE-12 and RDE-1 may also interact. Finally, RDE-12 failed to interact in IP and immunoblot analysis with FLAG::WAGO-6, another cytoplasmic WAGO (Figure 1G).

rde-12 Mutants Are Partially Defective in RNAi

To examine the function of *rde-12*, we obtained deletion alleles (*tm3644 and tm3679*) from the National Bioresource Project for the Experimental Animal "Nematode *C. elegans*" [13]. Immunoblot analysis failed to detect a protein in *rde-12(tm3644)* extracts and detected a protein of lower molecular weight in extracts from *rde-12(tm3679)* (Figure 1B). Animals homozygous for both alleles were viable and showed no obvious developmental defects. In dsRNA feeding assays with several triggers, both *rde-12* mutant strains were strongly, but not completely, resistant to RNAi targeting the muscle-specific gene *unc-22* and the essential gene *cpsf-2* (Figure 2B). This incomplete RNAi deficit was more apparent in assays targeting the germline gene *pos-1*. We found that 63% of *rde-12(tm3644)* and 89% of *rde-12(tm3679)* embryos were sensitive to *pos-1(RNAi)* (Figure 2B). Together with the immunoblot analysis, these findings suggest that *tm3644* is a strong loss-of-function (probably null) allele, while *tm3679* may retain partial function.

[4]Present address: Department of Cell Biology and Neuroscience, University of California, Riverside, Riverside, CA 92521, USA
*Correspondence: craig.mello@umassmed.edu

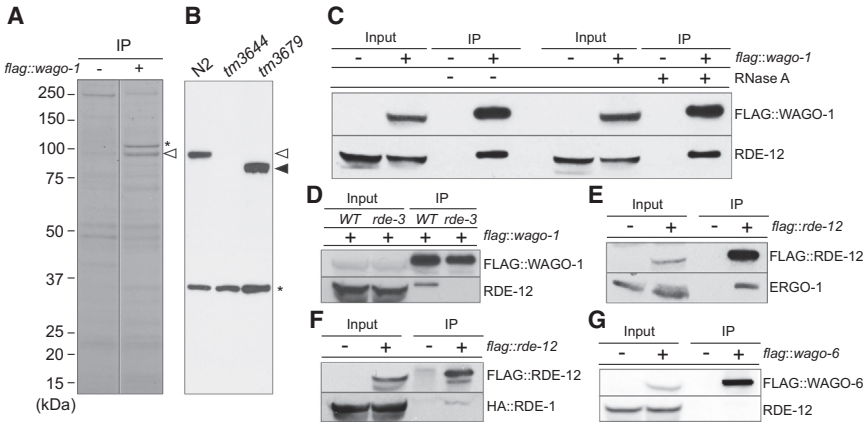

Figure 1. RDE-12 Binds to Both Primary and Secondary Argonautes

(A) Identification of FLAG::WAGO-1-interacting proteins. FLAG::WAGO-1 immune complexes from N2 wild-type (−) and *flag::wago-1* transgenic worms (+) were resolved on a denaturing polyacrylamide gel, and proteins were visualized by colloidal blue staining. FLAG::WAGO-1 is indicated with an asterisk, and a prominent 100 kDa interacting protein is indicated with an open arrowhead.

(B) Specificity of RDE-12 antisera. Immunoblot analysis with RDE-12-specific antisera on extracts from wild-type (N2), *rde-12(tm3644)*, and *rde-12(tm3679)* animals. The open and closed arrowheads indicate the expected mobility of RDE-12 produced in wild-type and *tm3679* animals, respectively. The asterisk indicates a background band.

(C–G) RDE-12 interactions with AGO proteins. Immunoblot analyses of FLAG IP experiments to monitor RDE-12 interactions with FLAG::WAGO-1 in the presence (+) or absence (−) of RNase A (C), FLAG::WAGO-1 in the wild-type (WT) and *rde-3* mutant (D), ERGO-1 (E), HA::RDE-1 (F), and FLAG::WAGO-6 (G) lysates. *flag* transgenic lysates are indicated by a + in the headings above the blots. The protein blotted by the antibody probes used in each experiment is indicated to the right of each blot.

The *rde-12(tm3644)* RNAi-deficient phenotype was rescued by both FLAG- and GFP-tagged RDE-12 transgenes (Figure 2B). Interestingly, the overexpression of *rde-12* in muscle from the *myo-3* promoter not only rescued the Rde phenotype of *tm3644*, but also enhanced the sensitivity of the transgenic animals to *unc-22* RNAi. Wild-type, nontransgenic animals exposed to *unc-22(RNAi)* produced 100% twitching progeny, but only 14% (n = 36) showed the most severe paralyzed twitching phenotype. Strikingly, the percentage of paralyzed animals increased to 72% (n = 29) for *myo-3::flag::rde12* transgenic animals among 100% twitching progeny, suggesting that the overexpression of RDE-12 enhances RNAi in the muscles.

To determine whether the ATPase activity in RDE-12 is required for its function, we generated an *rde-12* transgene construct bearing a lesion within motif I in the conserved lysine residue (K429A), which is required for ATP hydrolysis in DEAD box proteins [14] (Figure 2A). On the basis of GFP fluorescence (Figure S1A available online) and by immunoblotting with FLAG-specific antibodies (data not shown), we found that the expression of RDE-12(K429A) was identical to the expression of similarly tagged wild-type protein. Importantly, we found that RDE-12(K429A) was unable to rescue the RNAi deficiency of *rde-12(tm3644)* (Figure 2B), indicating that the ATPase activity of RDE-12 is essential for function.

rde-12 Mutants Are Sensitive to Viral Infection

The exo-RNAi pathway in *C. elegans* is an antiviral pathway [15, 16]. To ask whether *rde-12* mutants are defective in viral suppression, we exposed animals to Orsay virus [17]. We found that both *rde-12* mutant strains (*tm3644* and *tm3679*) exhibited dramatically increased viral-RNA levels relative to the wild-type, comparable in the case of *tm3644* to the levels observed in *rde-1(ne300)* mutants (Figure 2C). These findings suggest that RDE-12 functions in the antiviral response in *C. elegans*.

Primary and Secondary Argonaute Pathways Are Uncoupled in *rde-12* Mutants

During exoRNAi, RDE-1 engages primary sense and antisense siRNAs produced by the Dicer-mediated processing of the dsRNA trigger [9]. Once RDE-1 engages target mRNAs, secondary siRNAs, which are exclusively antisense, are produced by RdRP-dependent amplification [9, 18, 19]. To identify which step(s) of the RNAi pathway is compromised in *rde-12* mutants, we examined the level of primary and secondary siRNAs in mutant animals exposed to RNAi. To ask whether the production of primary siRNA and loading onto RDE-1 requires RDE-12 activity, we examined animals expressing a short hairpin RNA targeting the *unc-22* gene [19]. We found that the total level of siRNA produced from this transgene was similar in wild-type and *rde-12* mutant animals (Figure 2D). Furthermore, northern blot analysis of RDE-1 IP indicated that the level of *unc-22* siRNA loaded onto RDE-1 in the *rde-12* mutant was similar to or higher than the level observed in the wild-type (Figure 2D).

To ask whether RDE-12 is required for RdRP-dependent secondary siRNAs, we exposed animals to *cpsf-2* dsRNA and used northern blot analysis to detect secondary siRNAs that accumulate immediately upstream of the trigger dsRNA region in wild-type animals. Strikingly, this analysis revealed that secondary siRNAs were strongly depleted in *rde-12* mutants (Figure 2E). Deep sequencing of small RNAs from *cpsf-2(RNAi)* animals revealed a robust accumulation of primary siRNAs in *rde-12* mutants: sense siRNA levels under the trigger dsRNA region were similar in *rde-12* and wild-type animals (compare the upper and lower graphs in Figure 3A). However, antisense small RNA levels within this region and upstream of the trigger were reduced dramatically in *rde-12* mutants (Figure 3A and 3B), consistent with a defect in secondary siRNA biogenesis. Taken together, these findings are consistent with a role for RDE-12 downstream of primary siRNA biogenesis and RDE-1 loading, but upstream of secondary siRNA (22G-RNA) production and/or WAGO loading.

We also analyzed endogenous siRNA (endo-siRNA) accumulation in *rde-12* mutants. A variety of small RNA species are produced in at least seven different AGO pathways in *C. elegans* [4, 12, 20–27]. We found that the majority of small RNA species in these pathways were largely unaffected in *rde-12* mutants (Figure 3C and data not shown). In contrast, although the 26G-RNAs that bind to ERGO-1 were largely unaffected, we found that ERGO-1-dependent 22G-RNAs were strongly depleted in *rde-12* mutant animals (Figures 3C, 3D, and S2, and Table S1). Similarly, the only verified endogenous RDE-1 target, *y47h10a.5* [22], was strongly depleted of

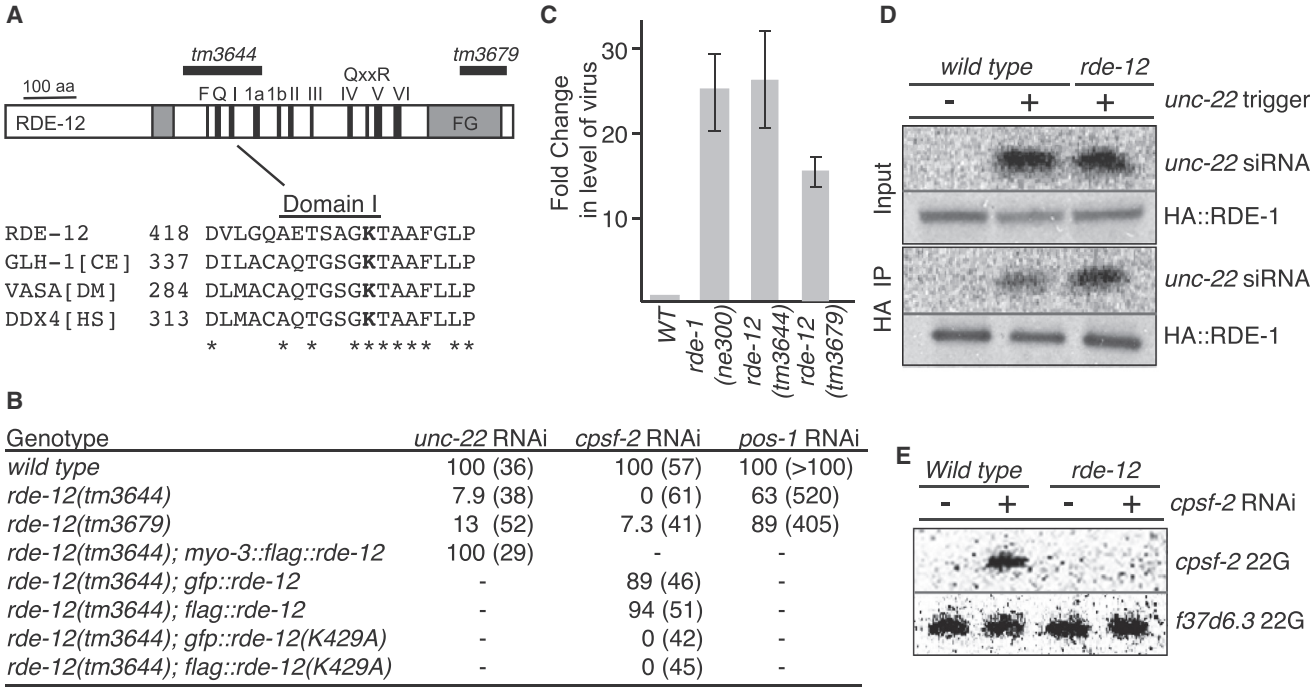

B

Genotype	*unc-22* RNAi	*cpsf-2* RNAi	*pos-1* RNAi
wild type	100 (36)	100 (57)	100 (>100)
rde-12(tm3644)	7.9 (38)	0 (61)	63 (520)
rde-12(tm3679)	13 (52)	7.3 (41)	89 (405)
rde-12(tm3644); myo-3::flag::rde-12	100 (29)	-	-
rde-12(tm3644); gfp::rde-12	-	89 (46)	-
rde-12(tm3644); flag::rde-12	-	94 (51)	-
rde-12(tm3644); gfp::rde-12(K429A)	-	0 (42)	-
rde-12(tm3644); flag::rde-12(K429A)	-	0 (45)	-

Figure 2. RDE-12 Is a DEAD-Box ATPase Required for RNAi and Viral Infection

(A) Schematic diagram of the predicted domain structure of RDE-12 protein. The approximate positions of 11 conserved motifs (F–VI) found in the RNA helicase domain are indicated (black boxes), as are two FG/GF-rich domains (gray boxes). The region deleted by a putative null allele, *rde-12(tm3644)*, and by a less severe deletion allele, *rde-12(tm3679)*, are indicated by the black bars above the diagram. An alignment of domain I from RDE-12 and related *C. elegans* (CE), *Drosophila melanogaster* (DM), and *Homo sapiens* (HS) proteins is provided below the diagram. Invariant amino acids are indicated with an asterisk (below), and the conserved lysine mutated in RDE-12(K429A) is indicated in bold.

(B) *rde-12(tm3644)* is deficient in RNAi. Wild-type, *rde-12(tm3644)*, *rde-12(tm3679)*, and transgenic animals (as indicated) were assayed for sensitivity to RNAi by feeding. The percent of *unc-22* twitching and/or paralyzed, the *cpsf-2* sterile, or the *pos-1* dead embryo phenotypes among (n) animals analyzed is shown.

(C) *rde-12* mutants are sensitive to virus infection. qRT-PCR analysis to measure the relative levels of Orsay virus RNA in N2 wild-type (WT), *rde-1(ne300)*, *rde-12(tm3644)*, and *rde-12(tm3679)* animals infected with Orsay virus. The fold change relative to wild-type-infected worms is indicated in $\log_2$ scale. Error bars indicate the SD calculated from three biological replicates.

(D) *rde-12* is not required for production and/or RDE-1-loading of primary siRNAs. Northern blots and immunoblots were probed for *unc-22* siRNA and HA::RDE-1, respectively. RNA and protein extracts were prepared from wild-type and *rde-12(tm3644)* mutant animals before (Input) and after IP with HA::RDE-1 (HA IP). The presence (+) or absence (−) of a transgene driving an *unc-22* hairpin dsRNA trigger is indicated.

(E) Secondary siRNAs fail to accumulate in *rde-12* mutants. Northern blot analysis of small RNAs isolated from wild-type and *rde-12(tm3644)* mutant animals fed with bacteria expressing *cpsf-2* dsRNA (+) or a control feeding vector (−) is shown. A *cpsf-2*-specific probe located upstream of trigger sequence (red bar below the gene structure in Figure 3A) was used to detect *cpsf-2* 22G-RNAs. An *f37d6.3*-specific probe was used to detect *rde-12*-independent endo-22G-RNAs.

secondary siRNAs in *rde-12* mutants (Figures 3E and 3F and Table S1). These findings suggest that RDE-12 is required for the production or stability of 22G-RNAs downstream of RDE-1 and ERGO-1.

RDE-12 Is Recruited to the Target RNA in an RDE-1-Dependent Manner

Although sequence-specific RNA binding has not been demonstrated for the majority of DEAD box proteins, they can be recruited to specific target RNAs by interacting with sequence-specific RNA-binding cofactors [28]. We therefore asked whether RDE-12 is recruited to target mRNA during RNAi. To test this possibility, we immunoprecipitated RDE-12 from animals exposed to dsRNA targeting the abundantly expressed *sel-1* mRNA and then measured *sel-1* mRNA in the RDE-12 immune complexes by quantitative RT-PCR (qRT-PCR) using primers upstream of the trigger dsRNA. This analysis revealed a *sel-1(RNAi)*-dependent interaction between RDE-12 and *sel-1* mRNA. Despite the fact that *sel-1* mRNA levels were reduced by 71% by *sel-1(RNAi)*, we observed a 6-fold enrichment of *sel-1* mRNA in RDE-12 coIP assays relative to levels detected in experiments on control animals exposed to empty vector (Figure 4A). The interaction between RDE-12 and the *sel-1* target mRNA was reduced in *rde-1(ne300)* mutants (Figure 4A). Taken together with our AGO coIP studies, these findings support the idea that RDE-1 (and perhaps ERGO-1) interacts with and recruits RDE-12 to target mRNA.

RDE-12 Localizes to Germline P Granules and to Similar, though Smaller, Perinuclear Cytoplasmic Foci in Somatic Cells

A previous study showed that RDE-12 C-terminally tagged with GFP (RDE-12::GFP) localizes to germline P granules and colocalizes with nuclear pore components [10]. We confirmed the P granule localization and nuclear pore association of RDE-12 using GFP::RDE-12 (Figures 4B–4D and S1A). GFP::RDE-12 localized throughout the cytoplasm and in perinuclear foci and colocalized prominently with P granules (PGL-1::mRFP [29]) in the germline (Figures 4B and S1A).

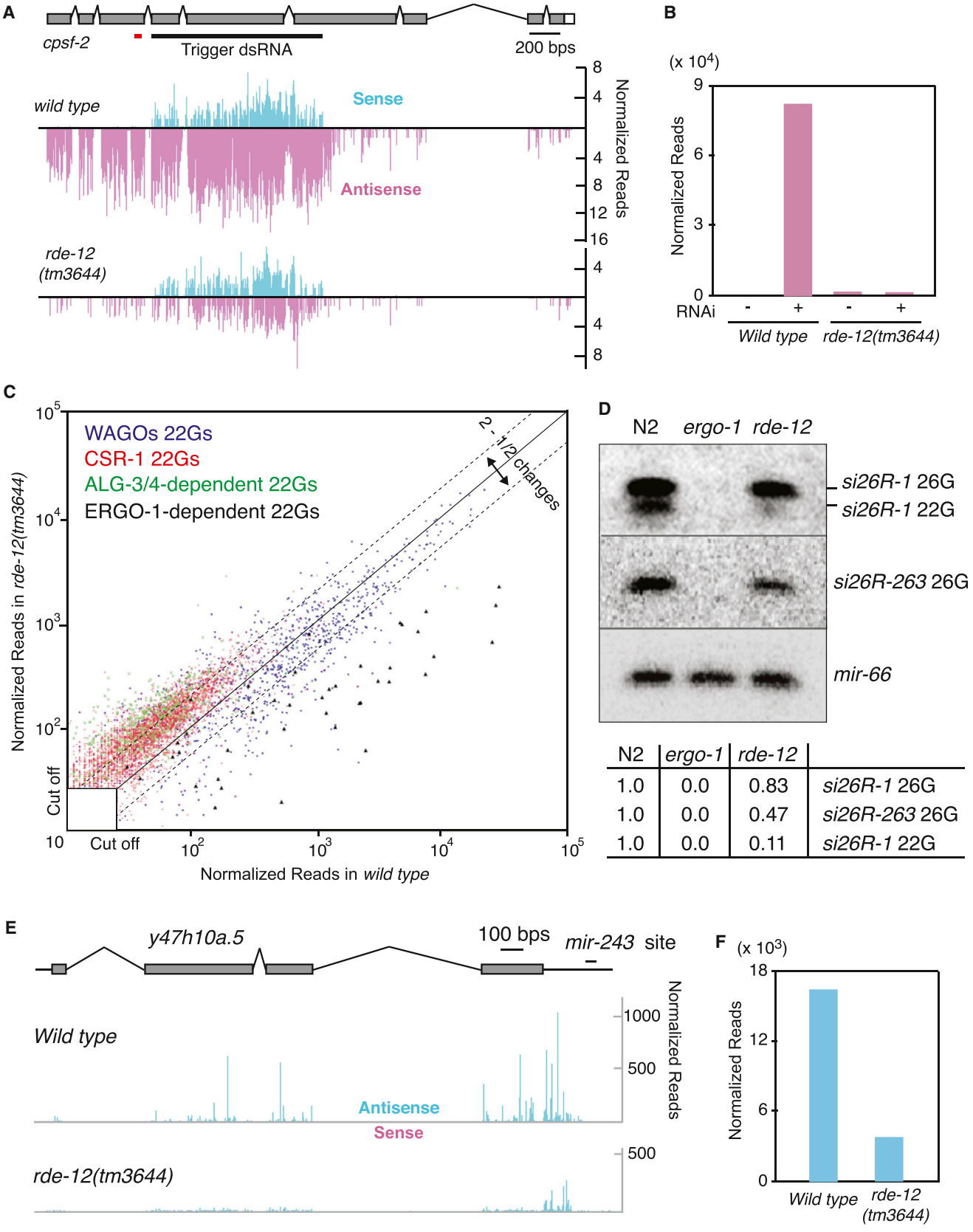

Figure 3. *rde-12* Is Required for 22G-RNA Accumulation in the RDE-1 and ERGO-1 Pathways

(A and B) *rde-12* is required for secondary 22G-RNA accumulation during exo-RNAi.

(A) Genome browser view showing the *cpsf-2* gene structure aligned above deep-sequencing read-density plots of the *cpsf-2* small-RNAs from wild-type and *rde-12(tm3644)* mutant strains exposed to *cpsf-2(RNAi)*. Sense reads (light blue) are indicated above the line, and antisense reads (pink) are indicated

(legend continued on next page)

Confocal microscopy revealed that perinuclear GFP::RDE-12 foci in somatic cells sometimes overlap with nuclear pores stained with a nucleoporin-specific antibody (Figures 4C and 4D and Movies S1 and S2). The cytoplasmic (nonperinuclear) RDE-12 foci in somatic cells appear to be similar to cytoplasmic processing bodies, or P bodies, which function in mRNA turnover [30]. However, we found that GFP::RDE-12 did not significantly colocalize with the P body marker mCherry::PATR-1 [31] (Figure 4E). We speculate that the somatic GFP::RDE-12 foci represent structures that are analogous to, albeit smaller than, germline P granules.

A recent study identified distinct cytoplasmic structures termed "mutator foci" [32] that are adjacent to, or partially overlap with, P granules and contain many factors required for the amplification of secondary siRNAs, including the cellular RdRP RRF-1 and the beta-nucleotidyltransferase RDE-3 [32]. We noted that GFP::RDE-12, like other P granule components, partially overlapped with mutator foci (Figure S1B). The germline localization of RDE-12 was similar to that of GFP::WAGO-1 [4], suggesting that the physical association of RDE-12 and WAGO-1 may occur in P granules. However, localization of GFP::WAGO-1 in P granules is not dependent on RDE-12 (data not shown).

Here we have identified the Vasa homolog RDE-12 as an AGO-interacting protein required for RNAi in *C. elegans.* The interaction between Vasa-related RNA-binding ATPases and Argonautes appears to be evolutionally conserved. In *Drosophila*, Vasa has been reported to interact with Aubergine (Aub), a Piwi subfamily protein that binds germline Piwi-interacting RNAs (piRNAs) [33], while Belle, a close paralog of Vasa, interacts with *Drosophila* Ago2 and appears to function with AGO2 in promoting chromosome segregation [34]. MVH, a mouse homolog of Vasa, associates with the Piwi Argonautes Miwi and Mili [35]. Vasa and Belle have been implicated in the piRNA, endo-siRNA, and miRNA pathways [36–38], but their specific biochemical functions in these pathways remain unclear.

We found that RDE-12 is required downstream of the primary AGOs RDE-1 and ERGO-1 for the accumulation of RdRP-dependent 22G-RNAs. Previous reports have shown that the RDE-10/RDE-11 complex is also essential for the amplification of secondary siRNA in both pathways [39, 40]. Perhaps, once loaded on the target mRNA, RDE-10/RDE-11 and RDE-12 signal downstream to recruit RdRP or other factors, such as RDE-3, that ensure efficient secondary small RNA (22G-RNA) accumulation (see the model in Figure 4F). We identified RDE-12 as a protein that interacts robustly with WAGO-1, a secondary AGO that engages 22G-RNAs downstream of RdRP amplification. Interestingly, the association of RDE-12 with WAGO-1 required RDE-3 activity, raising the possibility that the association of RDE-12 with WAGO-1 may occur on target mRNAs after 22G-RNA biogenesis and/or WAGO-1 loading. One attractive possibility is that RDE-12 functions on the target mRNA to promote loading of nascent 22G-RNAs onto WAGO-1. Perhaps RDE-12 dissociates from the target mRNA together with the newly loaded WAGO-1/22G-RNA RISC and, through its FG-repeat domains, positions WAGO-1 RISC in close proximity to the nuclear pore, where it is thus poised to scan mRNAs exiting the nucleus (Figure 4F).

WAGO-1, like other WAGOs, lacks key metal-coordinating residues in its RNase H-related PIWI domain [9], raising important questions regarding how WAGO-1 promotes silencing and whether WAGO-1 RISC is recycled for subsequent targeting events. It is possible that RDE-12 also functions in one or both of these downstream activities (Figure 4F). Further analysis of how RDE-12 binds to target mRNA and interacts with WAGO-1 during RNAi should shed light on the fascinating role of this and other DEAD box proteins in AGO-mediated mRNA surveillance.

Experimental Procedures

Genetics

All *C. elegans* strains were derived from the Bristol N2 strain and cultured as described [41]. The strains used in this study are listed in the Supplemental Experimental Procedures.

RDE-12 Antibodies

RDE-12 antibodies were affinity purified from rabbit antiserum raised against a synthetic peptide corresponding to residues 12–29 (GREYH DDRSNRDHRHGNG) of RDE-12.

Immunoblot Analysis

Antibodies used for immunoblotting include anti-RDE-12 (1/1000), anti-ERGO-1 (1/1000; [12]), anti-PRG-1 (1/1000; [26]), anti-CSR-1 (1/1000; [20]), anti-FLAG (1/1000; M2, Sigma), and anti-HA (1/4000; ab9110, Abcam).

RNA and Northern Blot Analysis

RNA purification and northern blot analysis were performed as described [4, 42].

Immunostaining

Embryos were dissected from worms directly on poly-L-lysine-coated glass slides and fixed as described (http://www.wormatlas.org/images/earlyembstaining.pdf).

below the line. The height of each bar indicates the frequency ($\log_2$ scale) of small RNAs that initiate at that genomic coordinate. The black bar below the gene structure indicates the location of the *cpsf-2* trigger dsRNA. The red bar below the gene structure indicates the probe used in Figure 2E.

(B) Bar graph analysis of the data in (A) indicating the normalized numbers of antisense siRNA reads mapping outside of the dsRNA trigger in wild-type and *rde-12(tm3644)* mutant animals with (+) or without (−) exposure to *cpsf-2* dsRNA.

(C and D) RDE-12 is required for ERGO-1 pathway 22G-RNAs.

(C) Scatterplot analysis of endo-siRNAs in the wild-type and *rde-12(tm3644)* mutants. Each point represents a previously defined locus (or gene) targeted by 22G-RNAs that depend on each of four pathways as indicated by the color code. Deviations from the diagonal indicate, on a $\log_{10}$ scale, the enrichment (above the line) or depletion (below the line) in *rde-12(tm3644)* mutants relative to wild-type animals. Dashed lines indicate 2-fold change. The minimal read cutoff was 25 in this analysis.

(D) Northern blot analysis of ERGO-1 pathway primary, 26G-RNAs, and secondary, 22G-RNAs, in wild-type (N2), *ergo-1(tm1890)*, and *rde-12(tm3644)* mutants. The blot was analyzed with specific probes to detect *si26R-1* and its corresponding 22G-RNA, *si26R-263*, and the microRNA *mir-66* (as indicated). Quantification of the relative amounts of 22G-RNAs and 26G-RNAs normalized to *miR-66* in *rde-12* mutants compared to the wild-type is shown below.

(E and F) *rde-12* is required for RDE-1-dependent endo-siRNAs targeting *y47h10a.5*.

(E) Genome browser view showing *y47h10a.5* aligned above deep-sequencing read-density plots. Small RNA distributions in wild-type and *rde-12(tm3644)* mutant strains are indicated on a linear scale. Antisense reads are indicated in light blue and sense reads (though largely absent) in pink. The location of the *mir-243* target site (which triggers secondary 22G-RNA accumulation) is indicated above the 3′ untranslated region of the *y47h10a.5* gene.

(F) Bar graph analysis of the data in (E) indicating the normalized total numbers of antisense siRNA reads mapping to the *y47h10a.5* gene in the wild-type and *rde-12(tm3644)* mutants.

See also Figure S2 and Table S1.

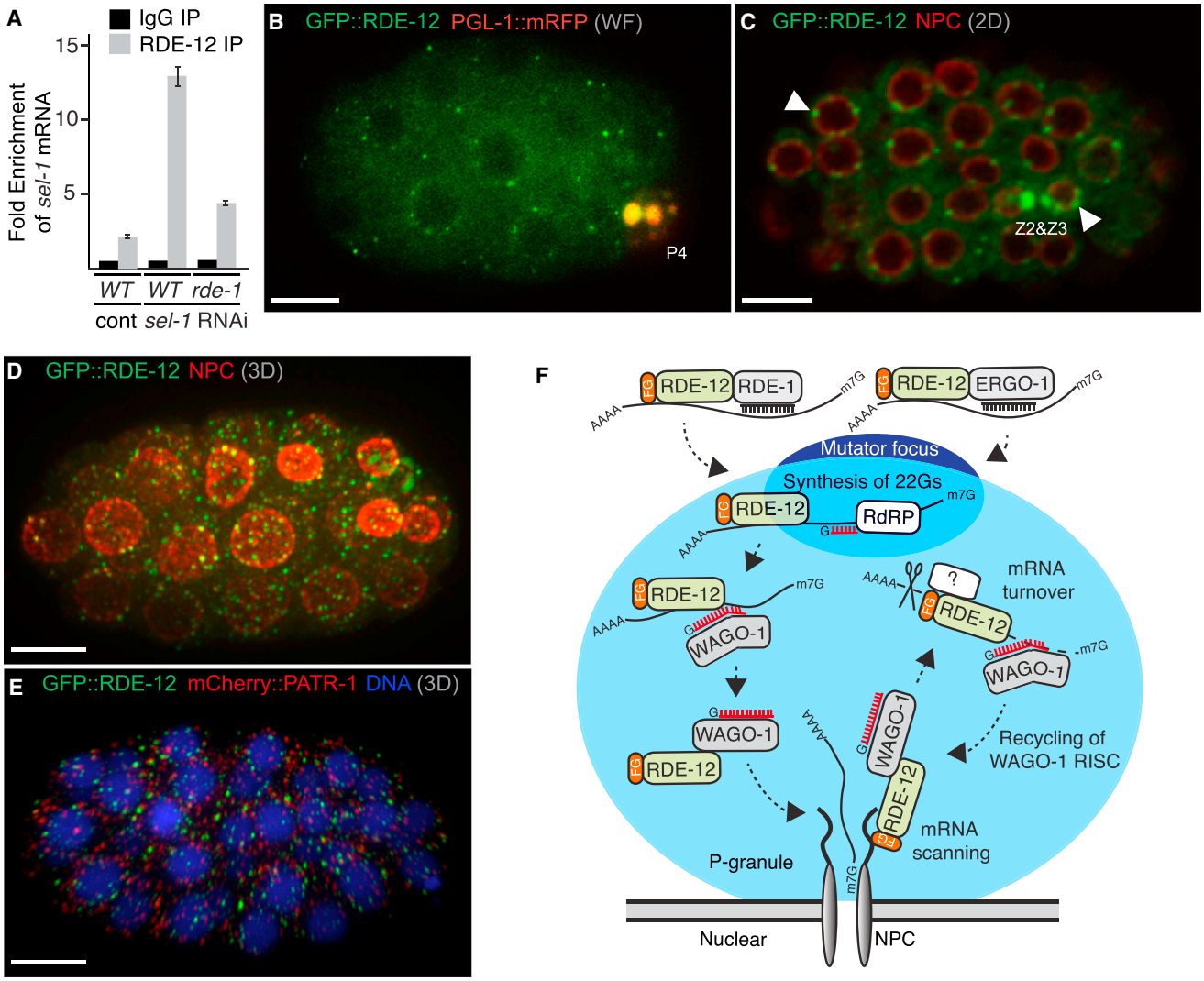

Figure 4. RDE-12 Binds Target mRNA during RNAi and Localizes to Cytoplasmic and Perinuclear Foci

(A) RDE-12 associates with target mRNA during RNAi. Bar graph showing qRT-PCR analysis of *sel-1* mRNA recovered from rabbit immunoglobulin G or RDE-12 IP from wild-type or *rde-1(ne300)* mutant lysates after control (cont) or *sel-1(RNAi)* (as indicated). Error bars indicate the SD calculated from three technical replicates.

(B) Fluorescence micrograph showing GFP::RDE-12 (green) is visible throughout the cytoplasm and in cytoplasmic and perinuclear foci, while PGL-1::mRFP (red) [29] is localized exclusively in the germline blastomere P4 (indicated). Colocalization in P4 appears (yellow) in this merged image.

(C and D) Confocal images of GFP::RDE-12 (green) and nuclear pore complexes (NPC; red) stained with GFP and nucleoporin-specific antibody mAb414, respectively. A single confocal section of an ~50-cell-stage embryo (C) shows cytoplasmic and perinuclear foci of GFP::RDE-12 in somatic cells and enriched in the two primordial germ cells (Z2 and Z3, indicated). Arrowheads show examples of perinuclear localization of GFP::RDE-12 in somatic and germ cells. A 3D projection of confocal images from a 24-cell-stage embryo is shown in (D).

(E) GFP::RDE-12 fails to colocalize with PATR-1. A 3D projection of confocal images from a 36-cell-embryo showing GFP::RDE-12 (green), mCherry::PATR-1 (red), and DNA (blue).

(F) Schematic model illustrating potential functions and interactions for RDE-12 during RNAi. A nuclear envelope and pore (NPC) are drawn at the base of the diagram with a P granule (light-blue sphere) docked above. A mutator focus (dark-blue sphere) is located in the top part of P granule, where secondary siRNAs are produced. RDE-12 is shown engaged at the pore through its FG domains. Dashed arrows indicate potential functions for RDE-12.

Scale bars represent 10 μm (B–E). See also Figure S1 and Movies S1 and S2.

Accession Numbers

Illumina data are available from the NCBI Gene Expression Omnibus under the accession number GSE54396.

Supplemental Information

Supplemental Information includes Supplemental Experimental Procedures, two figures, one table, and two movies and can be found with this article online at http://dx.doi.org/10.1016/j.cub.2014.03.008.

Acknowledgments

We thank Ho Yi Mak for sharing information prior to publication. We thank Paul Furcinitti for creating and processing confocal images, Shohei Mitani for *rde-12* deletion alleles, Hsin-Yue Tsai for help with RNA IP, and James Moresco and John Yates, III, for MudPIT analysis. We are grateful to the members of the Mello lab for input and discussion, especially Wen Tang and Heng-Chi Lee for their technical help with Orsay virus assays and IP and immunoblot, respectively, and Darryl Conte for comments on the text and figures. Some strains used in this study were obtained from the

Caenorhabditis Genetics Center. M. Seth is a Howard Hughes Medical Institute International Student Research Fellow. This work was supported by an NIH grant (GM058800) to C.C.M. C.C.M. is a Howard Hughes Medical Institute Investigator.

Received: January 22, 2014
Revised: February 27, 2014
Accepted: March 4, 2014
Published: March 27, 2014

References

1. Joshua-Tor, L., and Hannon, G.J. (2011). Ancestral roles of small RNAs: an Ago-centric perspective. Cold Spring Harb. Perspect. Biol. *3*, a003772.
2. Haley, B., and Zamore, P.D. (2004). Kinetic analysis of the RNAi enzyme complex. Nat. Struct. Mol. Biol. *11*, 599–606.
3. Hutvágner, G., and Zamore, P.D. (2002). A microRNA in a multiple-turnover RNAi enzyme complex. Science *297*, 2056–2060.
4. Gu, W., Shirayama, M., Conte, D., Jr., Vasale, J., Batista, P.J., Claycomb, J.M., Moresco, J.J., Youngman, E.M., Keys, J., Stoltz, M.J., et al. (2009). Distinct argonaute-mediated 22G-RNA pathways direct genome surveillance in the C. elegans germline. Mol. Cell *36*, 231–244.
5. Wilson, R.C., and Doudna, J.A. (2013). Molecular mechanisms of RNA interference. Annu. Rev. Biophys. *42*, 217–239.
6. Steiner, F.A., Okihara, K.L., Hoogstrate, S.W., Sijen, T., and Ketting, R.F. (2009). RDE-1 slicer activity is required only for passenger-strand cleavage during RNAi in Caenorhabditis elegans. Nat. Struct. Mol. Biol. *16*, 207–211.
7. Smardon, A., Spoerke, J.M., Stacey, S.C., Klein, M.E., Mackin, N., and Maine, E.M. (2000). EGO-1 is related to RNA-directed RNA polymerase and functions in germ-line development and RNA interference in C. elegans. Curr. Biol. *10*, 169–178.
8. Sijen, T., Fleenor, J., Simmer, F., Thijssen, K.L., Parrish, S., Timmons, L., Plasterk, R.H., and Fire, A. (2001). On the role of RNA amplification in dsRNA-triggered gene silencing. Cell *107*, 465–476.
9. Yigit, E., Batista, P.J., Bei, Y., Pang, K.M., Chen, C.C., Tolia, N.H., Joshua-Tor, L., Mitani, S., Simard, M.J., and Mello, C.C. (2006). Analysis of the C. elegans Argonaute family reveals that distinct Argonautes act sequentially during RNAi. Cell *127*, 747–757.
10. Sheth, U., Pitt, J., Dennis, S., and Priess, J.R. (2010). Perinuclear P granules are the principal sites of mRNA export in adult C. elegans germ cells. Development *137*, 1305–1314.
11. Chen, C.C., Simard, M.J., Tabara, H., Brownell, D.R., McCollough, J.A., and Mello, C.C. (2005). A member of the polymerase beta nucleotidyltransferase superfamily is required for RNA interference in C. elegans. Curr. Biol. *15*, 378–383.
12. Vasale, J.J., Gu, W., Thivierge, C., Batista, P.J., Claycomb, J.M., Youngman, E.M., Duchaine, T.F., Mello, C.C., and Conte, D., Jr. (2010). Sequential rounds of RNA-dependent RNA transcription drive endogenous small-RNA biogenesis in the ERGO-1/Argonaute pathway. Proc. Natl. Acad. Sci. USA *107*, 3582–3587.
13. Mitani, S. (2009). Nematode, an experimental animal in the national BioResource project. Exp. Anim. *58*, 351–356.
14. Caruthers, J.M., and McKay, D.B. (2002). Helicase structure and mechanism. Curr. Opin. Struct. Biol. *12*, 123–133.
15. Lu, R., Maduro, M., Li, F., Li, H.W., Broitman-Maduro, G., Li, W.X., and Ding, S.W. (2005). Animal virus replication and RNAi-mediated antiviral silencing in Caenorhabditis elegans. Nature *436*, 1040–1043.
16. Lu, R., Yigit, E., Li, W.X., and Ding, S.W. (2009). An RIG-I-Like RNA helicase mediates antiviral RNAi downstream of viral siRNA biogenesis in Caenorhabditis elegans. PLoS Pathog. *5*, e1000286.
17. Félix, M.A., Ashe, A., Piffaretti, J., Wu, G., Nuez, I., Bélicard, T., Jiang, Y., Zhao, G., Franz, C.J., Goldstein, L.D., et al. (2011). Natural and experimental infection of Caenorhabditis nematodes by novel viruses related to nodaviruses. PLoS Biol. *9*, e1000586.
18. Pak, J., and Fire, A. (2007). Distinct populations of primary and secondary effectors during RNAi in C. elegans. Science *315*, 241–244.
19. Sijen, T., Steiner, F.A., Thijssen, K.L., and Plasterk, R.H. (2007). Secondary siRNAs result from unprimed RNA synthesis and form a distinct class. Science *315*, 244–247.
20. Claycomb, J.M., Batista, P.J., Pang, K.M., Gu, W., Vasale, J.J., van Wolfswinkel, J.C., Chaves, D.A., Shirayama, M., Mitani, S., Ketting, R.F., et al. (2009). The Argonaute CSR-1 and its 22G-RNA cofactors are required for holocentric chromosome segregation. Cell *139*, 123–134.
21. Conine, C.C., Batista, P.J., Gu, W., Claycomb, J.M., Chaves, D.A., Shirayama, M., and Mello, C.C. (2010). Argonautes ALG-3 and ALG-4 are required for spermatogenesis-specific 26G-RNAs and thermotolerant sperm in Caenorhabditis elegans. Proc. Natl. Acad. Sci. USA *107*, 3588–3593.
22. Corrêa, R.L., Steiner, F.A., Berezikov, E., and Ketting, R.F. (2010). MicroRNA-directed siRNA biogenesis in Caenorhabditis elegans. PLoS Genet. *6*, e1000903.
23. Han, T., Manoharan, A.P., Harkins, T.T., Bouffard, P., Fitzpatrick, C., Chu, D.S., Thierry-Mieg, D., Thierry-Mieg, J., and Kim, J.K. (2009). 26G endo-siRNAs regulate spermatogenic and zygotic gene expression in Caenorhabditis elegans. Proc. Natl. Acad. Sci. USA *106*, 18674–18679.
24. Lee, H.C., Gu, W., Shirayama, M., Youngman, E., Conte, D., Jr., and Mello, C.C. (2012). C. elegans piRNAs mediate the genome-wide surveillance of germline transcripts. Cell *150*, 78–87.
25. Maniar, J.M., and Fire, A.Z. (2011). EGO-1, a C. elegans RdRP, modulates gene expression via production of mRNA-templated short antisense RNAs. Curr. Biol. *21*, 449–459.
26. Batista, P.J., Ruby, J.G., Claycomb, J.M., Chiang, R., Fahlgren, N., Kasschau, K.D., Chaves, D.A., Gu, W., Vasale, J.J., Duan, S., et al. (2008). PRG-1 and 21U-RNAs interact to form the piRNA complex required for fertility in C. elegans. Mol. Cell *31*, 67–78.
27. Grishok, A., Pasquinelli, A.E., Conte, D., Li, N., Parrish, S., Ha, I., Baillie, D.L., Fire, A., Ruvkun, G., and Mello, C.C. (2001). Genes and mechanisms related to RNA interference regulate expression of the small temporal RNAs that control C. elegans developmental timing. Cell *106*, 23–34.
28. Young, C., and Karbstein, K. (2012). Analysis of cofactor effects on RNA helicases. Methods Enzymol. *511*, 213–237.
29. Wolke, U., Jezuit, E.A., and Priess, J.R. (2007). Actin-dependent cytoplasmic streaming in C. elegans oogenesis. Development *134*, 2227–2236.
30. Parker, R., and Sheth, U. (2007). P bodies and the control of mRNA translation and degradation. Mol. Cell *25*, 635–646.
31. Gallo, C.M., Munro, E., Rasoloson, D., Merritt, C., and Seydoux, G. (2008). Processing bodies and germ granules are distinct RNA granules that interact in C. elegans embryos. Dev. Biol. *323*, 76–87.
32. Phillips, C.M., Montgomery, T.A., Breen, P.C., and Ruvkun, G. (2012). MUT-16 promotes formation of perinuclear mutator foci required for RNA silencing in the C. elegans germline. Genes Dev. *26*, 1433–1444.
33. Thomson, T., Liu, N., Arkov, A., Lehmann, R., and Lasko, P. (2008). Isolation of new polar granule components in Drosophila reveals P body and ER associated proteins. Mech. Dev. *125*, 865–873.
34. Pek, J.W., and Kai, T. (2011). DEAD-box RNA helicase Belle/DDX3 and the RNA interference pathway promote mitotic chromosome segregation. Proc. Natl. Acad. Sci. USA *108*, 12007–12012.
35. Kirino, Y., Vourekas, A., Kim, N., de Lima Alves, F., Rappsilber, J., Klein, P.S., Jongens, T.A., and Mourelatos, Z. (2010). Arginine methylation of vasa protein is conserved across phyla. J. Biol. Chem. *285*, 8148–8154.
36. Lim, A.K., and Kai, T. (2007). Unique germ-line organelle, nuage, functions to repress selfish genetic elements in Drosophila melanogaster. Proc. Natl. Acad. Sci. USA *104*, 6714–6719.
37. Zhou, R., Hotta, I., Denli, A.M., Hong, P., Perrimon, N., and Hannon, G.J. (2008). Comparative analysis of argonaute-dependent small RNA pathways in Drosophila. Mol. Cell *32*, 592–599.
38. Kotaja, N., Bhattacharyya, S.N., Jaskiewicz, L., Kimmins, S., Parvinen, M., Filipowicz, W., and Sassone-Corsi, P. (2006). The chromatoid body of male germ cells: similarity with processing bodies and presence of Dicer and microRNA pathway components. Proc. Natl. Acad. Sci. USA *103*, 2647–2652.
39. Yang, H., Zhang, Y., Vallandingham, J., Li, H., Florens, L., and Mak, H.Y. (2012). The RDE-10/RDE-11 complex triggers RNAi-induced mRNA degradation by association with target mRNA in C. elegans. Genes Dev. *26*, 846–856.
40. Zhang, C., Montgomery, T.A., Fischer, S.E., Garcia, S.M., Riedel, C.G., Fahlgren, N., Sullivan, C.M., Carrington, J.C., and Ruvkun, G. (2012). The Caenorhabditis elegans RDE-10/RDE-11 complex regulates RNAi by promoting secondary siRNA amplification. Curr. Biol. *22*, 881–890.
41. Brenner, S. (1974). The genetics of Caenorhabditis elegans. Genetics *77*, 71–94.
42. Duchaine, T.F., Wohlschlegel, J.A., Kennedy, S., Bei, Y., Conte, D., Jr., Pang, K., Brownell, D.R., Harding, S., Mitani, S., Ruvkun, G., et al. (2006). Functional proteomics reveals the biochemical niche of C. elegans DCR-1 in multiple small-RNA-mediated pathways. Cell *124*, 343–354.